Semi-Analytical Load Models Accounting for the Tilt and Motion of a Cylinder Impacted by a Plunging Breaking Wave

Paul Renaud, Florian Hulin, Marc Batlle Martin, Yves-Marie Scolan, Nicolas Jacques, Jeffrey C. Harris, Jean-François Filipot, Alan Tassin

Proceedings of the ASME 2023
42nd International Conference on Ocean, Offshore & Arctic Engineering
OMAE2023
June 11-16, 2023, Melbourne, Australia

DRAFT - OMAE2023-107740

SEMI-ANALYTICAL LOAD MODELS ACCOUNTING FOR THE TILT AND MOTION OF A CYLINDER IMPACTED BY A PLUNGING BREAKING WAVE

Paul Renaud[1,2,†,*], Florian Hulin[1,2,3,†] Marc Batlle Martin [1,4], Yves-Marie Scolan[2], Alan Tassin[3], Nicolas Jacques[3], Jeffrey C. Harris[4], Jean-François Filipot[1]

[1]France Energies Marines, Plouzané, France
[2]ENSTA Bretagne, CNRS UMR 6027, IRDL, Brest, France
[3]IFREMER, Plouzané, France
[4]LHSV, Ecole des Ponts, EDF R&D, Chatou, France

ABSTRACT

This work is part of the DIMPACT project that addresses breaking-wave-induced loads on floating wind turbines. In this context, the hydrodynamic impact of a strong plunging breaking wave on a cylinder is studied using semi-analytical models, with a focus on the loads sensitivity to the cylinder tilt and wave-cylinder relative motion.

Two semi-analytical models are applied in a strip theory approach under the Froude-Krylov assumption. A numerical wave is generated using a Fully Nonlinear Potential Flow (FNPF) solver, whose free surface geometry and kinematics feed the semi-analytical models. Semi-analytical slamming loads are compared with force measurements collected in a wave flume for different pitch angles and surge speeds. The temporal variation of the force as well as the maximum force acting on the cylinder are well estimated by the semi-analytical models. A new engineering formula is finally developed, accounting for the inclination and surge motion of the cylinder. The impact loads computed with this formula also show good agreement with the experimental tests.

Keywords: Plunging breaking wave, Wave loads, Slamming, Floating Offshore Wind Turbine (FOWT)

1. INTRODUCTION

Floating offshore wind turbines (FOWTs) can be subjected to high stresses during storms, such as slamming loads induced by breaking waves. Since the structure is floating, its inclination and dynamics must be taken into consideration when evaluating design loads.

The hydrodynamic impact induced by breaking waves on fixed vertical cylinders has been widely studied in recent years [1–4]. The emergence of new technologies such as FOWTs leads to adapt the existing models to take into account the dynamics of the structure.

The structure experiences motion due to the interactions with the waves. The hydrodynamic load acting on a moving body is generally studied by accounting for the relative kinematics between the flow and the structure [5, 6]. This will be extended to the partially immersed body. In particular, the semi-analytical "Composite Wagner-von Kármán Model" (denoted CWvKM hereafter) presented in [7] is adapted to account for the horizontal speed of the structure. Loads acting on inclined structures are generally estimated by accounting for the horizontal component of the fluid velocity in the body reference frame [8, p.225]. This is done presently.

Plunging breaking waves cause a strong impact on the structure. In the numerical simulations from [9], the wave crest of a plunging breaker separates from the cylinder at the rear of the cylinder. Flow separation can be modelled by using the Fictitious Body Continuation (FBC) [10]. This technique extends the Linearized Wagner Model (LWM) after flow separation. The FBC is implemented on the upper part of the body. On the lower part of the structure where there is no flow separation, the load model based on the Generalized von Kármán Model (GvKM) presented in [7] is used.

This work is part of the DIMPACT (Design of floating wind turbines and impacts of energetic steep and breaking waves) project. The present study is a follow-up to the DIMPACT test campaign [11]. The study investigates the ability of semi-analytical load models to capture the impact load caused by a strong plunging breaker on an instrumented cylinder. The cylinder is deployed in a wave flume under different tilt angles and surge motions. The wave geometry and kinematics required as input of the load models are provided by a FNPF solver.

The experimental campaign and its settings are discussed in section 2. Section 3 is dedicated to the formulations of the

[†]Joint first authors
[*]Corresponding author

two semi-analytical models, accounting for the orientation and surge speed of the structure. The loads predicted by the semi-analytical models and by engineering formulas are compared with the measured loads in section 6. A discussion regarding the governing parameters of the model based on the FBC is proposed in section 7. From the different observations of the semi-analytical models, a new simplified impact load formula that takes into account the inclination and the speed of the structure is elaborated.

2. EXPERIMENTAL CAMPAIGN

The experimental campaign conducted within the DIMPACT project is presented in [11]. The trials are at 1:25 scale.

2.1 Experimental setup

A segmented cylinder with a diameter of $D = 0.4\,m$ is mounted on a six degrees of motion hexapod in Ifremer's wave flume. An overview of the cylinder mounted below the hexapod is depicted in Fig. 1. The flume is $40.5\,m$ long from the wave generator to the absorbing beach, $2\,m$ deep, $4\,m$ wide and it is equipped with a segmented piston-type wave generator. The zone of the cylinder on which the wave impacts is composed of four instrumented sections. The sections are numbered from 1 to 4. Section 1 is the highest section and section 4 the lowest. Each of the sections is $15\,cm$ high and is composed of an external part linked to the backbone of the cylinder through a 4-axis load cell (torque and force are measured along the two horizontal directions). The force is thus measured independently on the different sections. The cylinder is extended below and above the instrumented sections to mimic the flow developing along an infinite cylinder. The complete cylinder is $1.81\,m$ high. Further details on the mockup are available in [11].

FIGURE 1: OVERVIEW OF THE CYLINDER, THE HEXAPOD AND THE FLUME.

2.2 Generation of the breaking wave

Breaking waves were generated numerically before being generated in the wave flume. This eases the process of adjusting the position of breaking. Ifremer's wave flume and its piston-type wave generator are modelled using a Fully Non-Linear Potential Flow solver (FNPF) based on the Boundary Element Method (BEM). The FNPF solver is described in [12] and [13]. Breaking waves are generated through the focalisation of a truncated JONSWAP spectrum. Non-linear effects induce a shift of the breaking point with respect to the focusing point. The focusing point is iteratively adjusted so that the wave breaks at the desired location [11].

In this study, we focus on one particular plunging breaking wave. It is generated through the focalisation of a JONSWAP spectrum in which only the low-frequency components are kept (cut-off frequency at $0.8\,Hz$). A frequency discretization of $0.01\,Hz$ is used. The peak period is $2.25\,s$, the significant wave height $0.15\,m$ and the peak enhancement factor 3.3. The non-dimensional depth of the flume is $kd = 1.7$, where k is the wave number associated with the spectrum peak period. This corresponds to intermediate water depth.

The free surface profile of the wave is experimentally measured through the use of a high-speed video camera. The wave was generated before the structure was installed. The intersection between the water and the wall of the flume is filmed using a frequency of 50 fps. The points situated on the intersection are detected through the use of a Canny filter. A checkerboard is placed in the wall plane to convert the pixels detected on the intersection into their coordinates in the flume reference frame. Using this technique, we measured a crest speed of $2.98\ m.s^{-1}$ and a crest height of $0.37\ m$. A satisfactory agreement between the experimental and numerical wave profiles is obtained in terms of geometry and crest speed. For this reason, we will consider that the wave profile and kinematics obtained numerically are a good approximation of the experimental wave. The free surface shape and the wave kinematics obtained numerically are used to feed the load models.

2.3 Signal processing

The slamming events generate strong vibrations of the structure, resulting in high oscillations in the measured force. These oscillations are due to the elasticity of the load cell, of the instrumented sections and of the hanging frame. The load signals were low-pass filtered using a cutoff frequency of $300\,Hz$ to remove these oscillations. One should keep in mind that the filtering induces oscillations at the cutoff frequency before and after the peak load due to the so-called Gibb's phenomenon. The high-frequency content of the load is also removed by the process.

3. SEMI-ANALYTICAL WAVE LOAD MODELS

Two semi-analytical models are proposed here describing the progressive immersion of a moving cylinder in a breaking wave. The models are applied in a strip-theory approach, considering the free surface and kinematics unaffected by the structure (Froude-Krylov assumption). In the first model, it is assumed that the wetted surface keeps expanding after the impact. The added mass of the body increases with the penetration depth into the fluid. In the second model, flow separation is taken into consideration. The relative kinematics between the body and the wave is accounted for.

3.1 CWvKM for a moving body

The first model is the Composite Wagner-von Kármán Model described in [7]. This model is based on the continuity of the added mass as a function of the immersion of the body in the fluid. At the first instants of penetration, the pressure from the Modified Logvinovich Model (MLM) [14] in the version presented in [10, 15] is integrated on the wetted surface of the body. The added mass computed with the MLM is then related to the added mass predicted within the frame of the Generalized von Kármán Model [16]. A linear transition between the added mass predicted by these two theories is defined. The transition starts from the penetration depth at which the FBC model predicts flow separation, h_{trans} [7]. The principle of the FBC method is represented in Fig. 2.

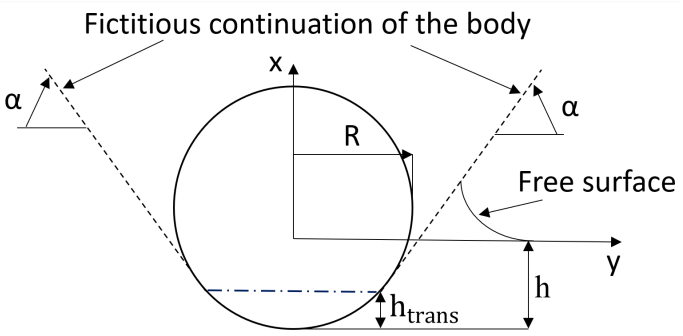

FIGURE 2: ILLUSTRATION OF THE FBC CONCEPT FOR THE VERTICAL WATER ENTRY OF A HORIZONTAL CYLINDER.

The fully non-linear flow kinematics of the wave computed with the FNPF solver is accounted for. The quadratic terms in the momentum equation are accounted for in the load model.The total distributed load acting on a strip of thickness dl as a function of the penetration depth h is:

$$dF_{tot}(h) = \left(\rho A(h)\frac{dU}{dt} + F_a(h)\left(\frac{dU}{dt} - \frac{dU_b}{dt}\right) + F_v(h)(U-U_b)^2 + F_a(h)(U-U_b)\frac{\partial W}{\partial z} + \frac{1}{2}\rho C_D(h) D (U-U_b)|U-U_b|\right)dl \quad (1)$$

where ρ is the fluid density, A is the immersed area, U the fluid velocity in the same direction as dF_{tot}, F_a is the added mass, U_b the horizontal speed of the body, $F_v(h)(U-U_b)^2$ represents the slamming term, W is the velocity perpendicular to U, C_D is the drag coefficient. The fluid acceleration accounts for convective terms:

$$\frac{dU}{dt} = \frac{\partial U}{\partial t} + U\frac{\partial U}{\partial x} + W\frac{\partial U}{\partial z} \quad (2)$$

The terms on the right hand-hand side of Eq. 1 represent the Froude-Krylov, added mass, slamming, axial divergence [17] and drag forces.

The Froude-Krylov force is only due to fluid inertia. It is not affected by body kinematics. The evolution of the hydrodynamic coefficients as a function of h involved in Eq. 1 are presented in [7]. The average kinematics on the strip is accounted for, from 0 to h.

3.2 FBC-based model - Flow separation modelling

A second semi-analytical model is presented. It is assumed that the flow separates over the upper part of the structure. We denote z as the vertical axis in the cylinder reference frame. The flow separates for $z > (1-\lambda)\eta_b$ with η_b the crest elevation and λ indicates the portion of the structure on which there is flow separation. This parameter can be seen as the commonly used "curling factor" in the engineering slamming formula.

The Wagner Model can be extended after flow separation by using the FBC model [10]. Straight lines with an angle α (see Fig. 2) are added to the geometry. The lines define a fictitious body surface on which the Wagner condition is applied. With $\alpha = 60°$, the slamming coefficient ($C_s = \frac{F}{\rho U^2 R}$) of a cylinder entering a flat free surface at constant speed is similar to the experimental slamming coefficient from [18] (referred to as "C&W") for large penetration depth. Separation occurs from $h = h_{trans}$.

The pressure from the MLM is integrated on the wetted surface. The term proportional to the velocity squared is integrated only on its positive support [see 10]. During the separation stage, there is no drag load since $C_D = 0$ for $h/R < 0.351$ [see 19]. The nonlinearity of the flow kinematics is accounted for up to second-order, as in the CWvKM.

It is assumed that there is no impact for $z < (1-\lambda)\eta_b$. The "quasi-static" load is then computed by using the GvKM described in [7]. The total distributed force $dF_{tot}(h)$ is given by:

if $z > (1-\lambda)\eta_b$:

$$dF_{tot}(h) = \left(\rho A(min(h, h_{trans}))\frac{dU}{dt} + F_a(h)\left(\frac{dU}{dt} - \frac{dU_b}{dt}\right) + F_v(h)(U-U_b)^2 + F_a(h)(U-U_b)\frac{\partial W}{\partial z}\right)dl \quad (3)$$

else:

$$dF_{tot}(h) = \left(\rho A(h)\frac{dU}{dt} + m_a(h)\left(\frac{dU}{dt} - \frac{dU_b}{dt}\right) + \frac{dm_a}{dh}(U-U_b)^2 + m_a(h)(U-U_b)\frac{\partial W}{\partial z} + \frac{1}{2}\rho C_D(h) D (U-U_b)|U-U_b|\right)dl \quad (4)$$

The terms F_a and F_v are given in [15] and m_a refers to the added mass predicted in the frame of the Generalized von Kármán's theory [16]. During the separation stage, the average kinematics on the strip from 0 to h_{trans} is taken into account.

When the strips are deeply immersed ($h > 4R$), the inertia load from the CWvKM and the GvKM returns to the formulation proposed by [6].

4. ACCOUNTING FOR ORIENTATION

The effect of the pitch angle θ is studied. The center of rotation is at the still water level, at the center of the cylinder. The rotation is positive clockwise (see Fig. 13 in [11]). When the structure is inclined, the velocity is expressed in the reference

frame of the cylinder. The horizontal velocity on the strip is accounted for. We denote the vector of fluid velocity in the reference frame (x, z) $\overrightarrow{U_{fluid}} = \begin{pmatrix} u_x \\ u_z \end{pmatrix}$. The horizontal fluid velocity on the strip is then $U = u_x \cos\theta - u_z \sin\theta$.

5. STRIP THEORY APPROACH

The models are implemented in a strip-theory approach, considering the free surface and kinematics undisturbed by the structure (Froude-Krylov assumption). The kinematics in the fluid is extracted from the FNPF solver, at points spaced 2 cm horizontally and vertically and then linearly interpolated in the domain. The mean kinematics on the strip is accounted for. Two geometrical modifications of the free surface are done:

- When the crest overturns, the extremity of the water jet may be lower than other points on the wavefront. The strip is wetted at the extremity but not in its middle preventing the assessment of the wetted surface. To circumvent this difficulty, the points of the water jet that make up the flipped part of the crest are removed, as illustrated in Fig. 3.

- The free surface is discretized. By linearly interpolating the points forming the free surface (see the Original free surface in Fig. 3), the wavefront is not well defined in the area where the radius of curvature is small. Since the slamming load is very sensitive to the penetration depth which is directly measured on the free surface, it could lead to inconsistencies. A quadratic interpolation is therefore performed to join the points in this specific area.

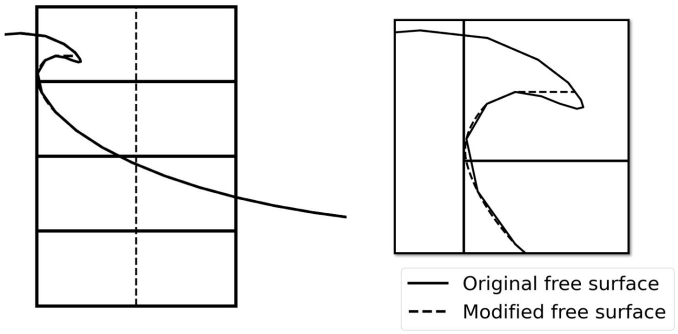

FIGURE 3: ILLUSTRATION OF THE GEOMETRICAL MODIFICATIONS MADE TO THE FREE SURFACE.

6. APPLICATIONS

We first investigate the differences between the proposed semi-analytical model on a fixed vertical cylinder. The parameter λ is calibrated. The load components of the FBC model are discussed. We then treat the inclined cylinder and finally we consider the moving cylinder.

6.1 Case 1: vertical and fixed cylinder (θ = 0 ; U_b = 0)

In this configuration, the cylinder is vertical and fixed. The loads in the four instrumented sections are compared. The parameter λ from the FBC-based model, which characterizes the height over which there is flow separation is set to 0.4 for plunging breakers. This value is commonly used in semi-analytical slamming load models [1, 2, 4, 20] for the curling factor (defining the portion of the wave contributing to the impact). This value will be discussed in section 7.

The load model presented in [21] is also implemented: when the section is partially immersed ($h < D$), the C&W formula is applied, then for $h > D$, the load is computed with the Morison equation ("M") with constant inertia ($C_m = 2$) and drag ($C_D = 1.2$) coefficients. This model is referred to as "C&W + M". Figure 4 compares the variation of the 3 theoretical forces to the experimental data in the four instrumented sections. The origin in time is centred at the instant of maximum load (T_{impact}).

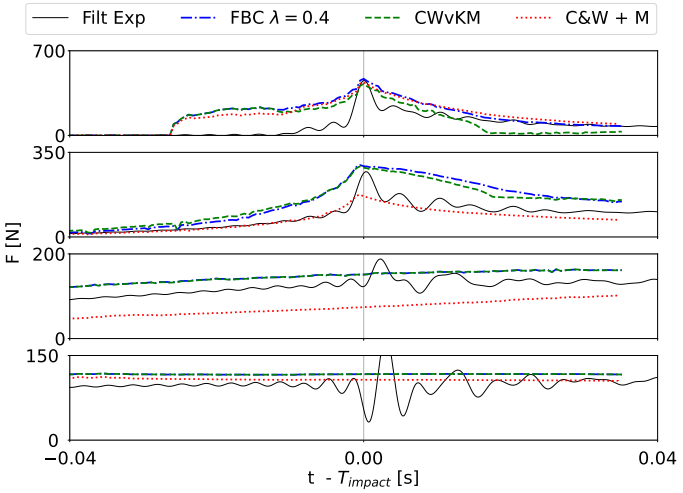

FIGURE 4: TIME HISTORY OF THE LOAD DECOMPOSED BY SECTION. FROM TOP TO BOTTOM: SECTION 1 TO 4. COMPARISON BETWEEN FILTERED EXPERIMENTAL DATA (FILT EXP, BLACK LINE) AND SEMI-ANALYTICAL RESULTS: FBC WITH λ = 0.4 (BLUE DASH-DOT LINE), CWVKM (GREEN DASH LINE), CAMPBELL & WEYNBERG FORMULA + MORISON EQUATION (C&W + M, RED DOTTED LINE). - θ = 0 ; U_b = 0

Good agreement is found in the two lower sections. The oscillations visible in the experimental curves in the two lower sections are due to the transmitted dynamic response of the two upper sections. Since the lower section is deeply immersed, the load models return to the Morison Fully Non-Linear model [22] with constant hydrodynamic coefficients. Section 3 is partially submerged. The load is correctly captured in this portion as well. The load predicted by the "C&W +M" model is lower than the experimental signal. Since a large portion of this segment is partially immersed, the load associated with the acceleration is not taken into account.

Section 2 is partially immersed too and is hit by the wavefront. There is no major difference between the two proposed semi-analytical models. The load increase is slightly overestimated by the present models. This can be explained by the run-up occurring in front of the cylinder. During the DIMPACT project, a Navier-Stokes (NS) solver is implemented to evaluate the hydrodynamic impact on a vertical cylinder [23]. Figure 5 shows the comparison of the free surface affected by the cylinder (3D) and the free surface without the structure (2D), both computed with the NS solver. The wave profile is greatly distorted in

front of the second section before the water jet hits the cylinder. This phenomenon may also appear during the experiments. It would explain the discrepancy during the load increase between the proposed models that take as input the undisturbed wave and the force measured in section 2.

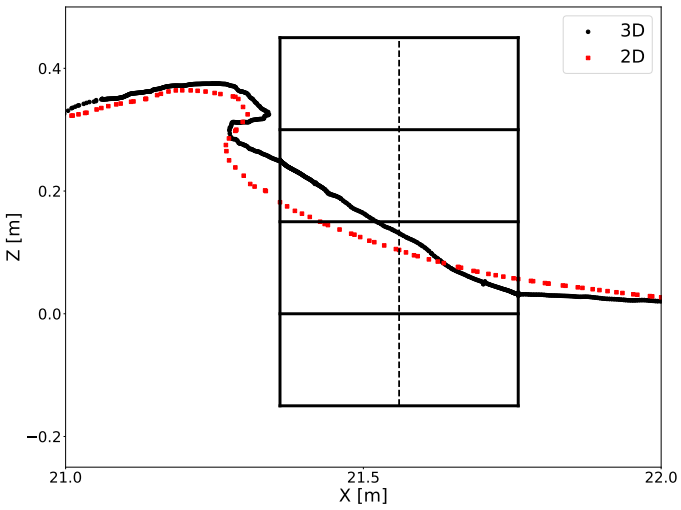

FIGURE 5: COMPARISON OF THE NUMERICAL FREE SURFACES COMPUTED WITH A NAVIER-STOKES SOLVER. THE "3D" FREE SURFACE ACCOUNTS FOR THE PRESENCE OF THE STRUCTURE.

On the one hand, the maximum force is better captured by the semi-analytical models than by using C&W formula. On the other hand, the force predicted by the proposed models after the impact is overpredicted. There are several reasons that could explain this difference:

- The slamming coefficient predicted by the integration of the MLM pressure is higher at the first instants of penetration than the experimental slamming coefficient from C&W [see 10]. Consequently, the maximum impact load is larger in the frame of the semi-analytical models.

- The load decay is well captured by using C&W formula which accounts for flow separation in the entire section. The semi-analytical models, on the other hand, slightly overpredict the load decay, suggesting that the height at which the flow separates may have been underestimated.

Figure 6 depicts the time variation of the load acting on section 2 estimated with the FBC-based model for various λ. On the one hand, the maximum load acting on this segment decreases by 10% as λ is increased. On the other hand, the force after the impact ($t - T_{impact} > 0.02$) is in better agreement with the experimental data for large values of λ. With $\lambda = 0.55$, the force predicted by the model fits the experimental results. This value is thus chosen for the rest of the study.

Section 1 is directly impacted by the jet of water as shown in Fig. 3. For $t - T_{impact} < 0$, a much higher load is computed with the models while high-frequency oscillations are present in the experimental load signal. One explanation could be that when the jet hits the cylinder, the splash spreads in all directions [2]. These strong 3D effects would lead to load overestimations when using the strip theory approach and the Froude-Krylov assumption. Furthermore, the experimental reconstruction of the

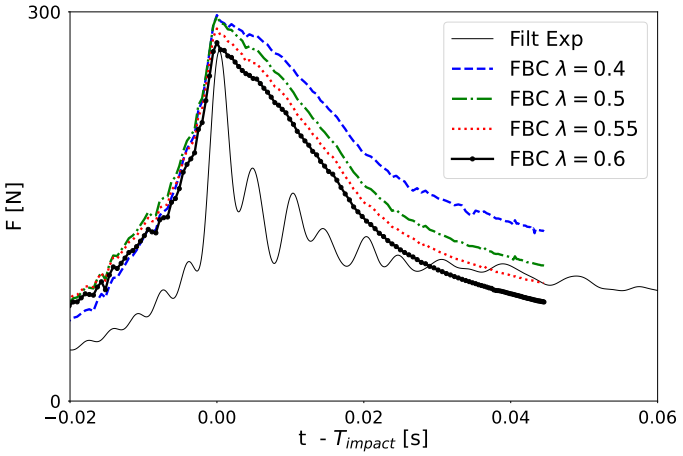

FIGURE 6: TIME HISTORY OF THE LOAD ACTING ON SECTION 2 COMPUTED WITH THE FBC-BASED MODEL USING DIFFERENT VALUES OF λ.

free surface shape after overturning is not possible due to the foam that hinders the contour detection algorithm. The jet also hides the free surface below it. We therefore have no means to check that the shape of the jet computed numerically is in good agreement with the physical jet shape. Moreover, the wave celerity is slightly higher in the experiment than in the numerical configuration [11]. The breaking stage of the numerical wave may therefore be later than in the experiment at the time of impact on the structure. This would explain the more developed water jet of the numerical wave.

The three models predict a similar maximum force in the upper section. However, the load decay is in better agreement when accounting for flow separation.

We propose to study separately the terms involved in the FBC-based model for the load acting above $z > (1-\lambda)\eta_b$. Each contribution is computed separately and depicted in Fig. 7. The AD and FK terms are proportional to the fluid acceleration. They represent respectively 8% and 1% of the total force. Therefore, it is justified to study the hydrodynamic impact at constant velocity. The AD term is negative and can represent about 15% of the load after the impact. The amplitude of this contribution is too large to be omitted to accurately predict the load decay. From Fig. 7, it can be seen that the maximum load is well estimated by the slamming term.

Finally, the force acting on the two upper sections is presented in Fig. 8. Engineering formulas from [1],[2] (denoted W&O hereafter) and [4] are implemented using a curling factor $\lambda = 0.55$ and a wave celerity $C = 2.87\,m.s^{-1}$ (following the time derivative of the horizontal position of the maximum of free surface elevation). W&O formula is strongly conservative, since it accounts for a uniform impact load, over the height $\lambda\eta_b$ using the phase speed C, within the frame of Wagner's theory ($C_s = 2\pi$). Furthermore, the ratio H_b/D, H_b being the wave height at breaking location, is significantly higher in W&O experiments ($H_b/D \in [3,4]$) than in the present configurations ($H_b/D \approx 1$). This could also explain the discrepancies using W&O formulation in the current study. Goda formula predicts a lower load than

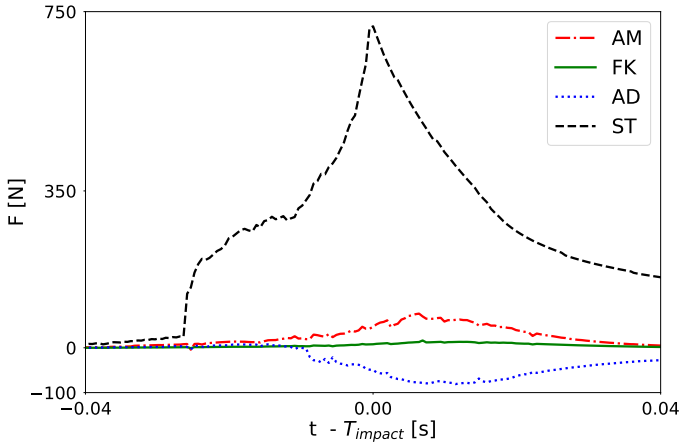

FIGURE 7: TIME HISTORY OF THE LOAD COMPUTED WITH THE FBC-BASED MODEL ($\lambda = 0.55$), DECOMPOSED BY COMPONENT. COMPARISON OF THE ADDED MASS TERM (AM, RED DASH-DOT LINE), THE FROUDE-KRYLOV TERM (FK, GREEN LINE), THE AXIAL DIVERGENCE TERM (AD, BLUE DOTTED LINE) AND THE SLAMMING TERM (ST, BLACK DASHED LINE).

W&O since von Kármán's theory is used ($C_s = \pi$). Formula from Paulsen provides a smooth time variation of the slamming load but predicts an underestimated impact load.

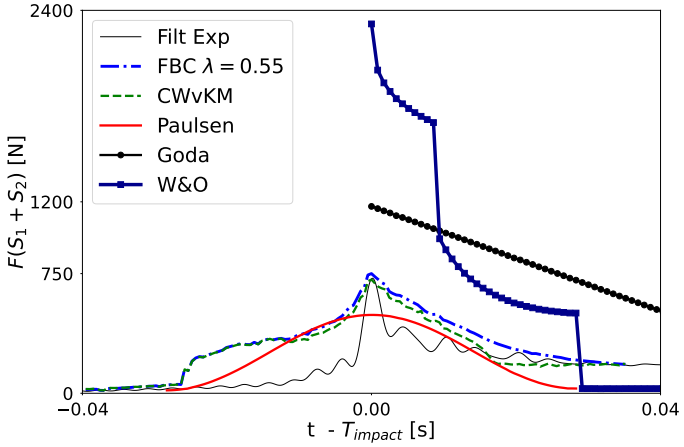

FIGURE 8: TIME HISTORY OF THE INLINE FORCE ACTING ON SECTIONS 1 & 2. COMPARISON BETWEEN FILTERED EXPERIMENTAL DATA (FILT EXP, BLACK LINE) AND SEMI-ANALYTICAL RESULTS: FBC WITH $\lambda = 0.55$ (BLUE DASH-DOT LINE), CWVKM (GREEN DASHED LINE), PAULSEN (RED LINE), GODA (CIRCLE MARKS) AND W&O (SQUARE MARKS).

6.2 Case 2: inclined and fixed cylinder ($\theta \neq 0$; $U_b = 0$)

The models are applied to an inclined cylinder. The pitch angle varies from $-10°$ to $10°$. Figure 9 shows the comparison of the load acting in each segment of the cylinder for $\theta = 5°$.

The semi-analytical models well capture the load acting on the two lower sections. We find the same overestimation of the force at the beginning of the impact in section 1. The maximum force is in good agreement as well. The load decay is still better estimated by the model based on the FBC in the two upper sections.

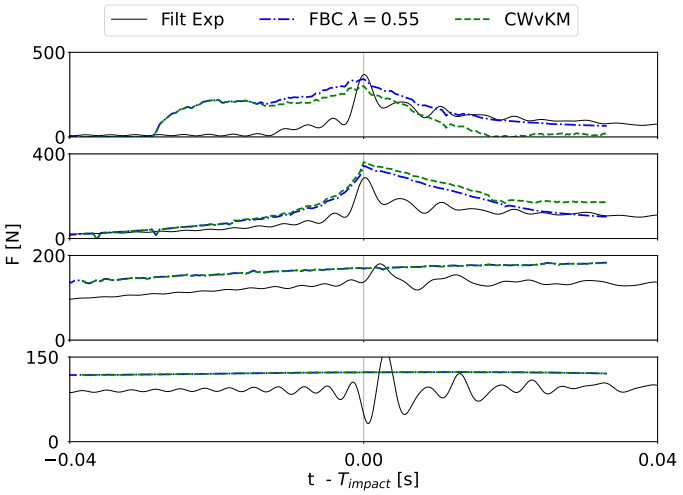

FIGURE 9: TIME HISTORY OF THE LOAD DECOMPOSED BY SECTION. FROM TOP TO BOTTOM: SECTIONS 1 TO 4. COMPARISON BETWEEN FILTERED EXPERIMENTAL DATA (FILT EXP, BLACK LINE) AND SEMI-ANALYTICAL RESULTS: FBC WITH $\lambda = 0.55$ (BLUE DASH-DOT LINE) AND CWVKM (GREEN DASHED LINE). - $\theta = 5°$; $U_b = 0$

Figure 10 shows the measured and the calculated load acting on the first two sections (where the impact occurs) as a function of the pitch angle. The mean relative discrepancies between the experimental data and the CWvKM and the FBC-based model are -2% and 4% respectively. The ability of the models in accounting for the structure's inclination is demonstrated.

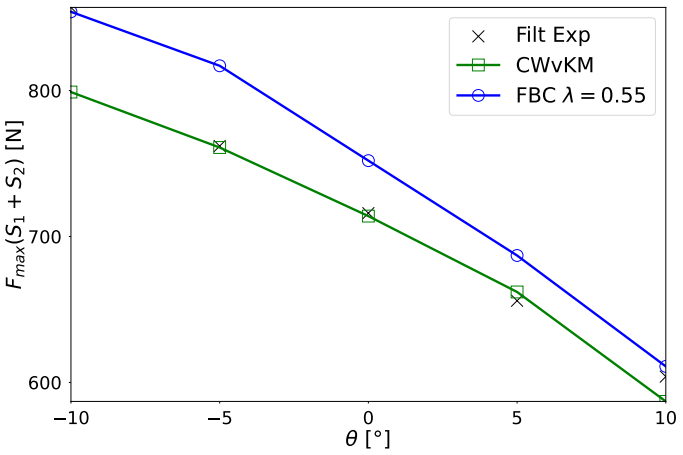

FIGURE 10: VARIATION OF THE MAXIMUM LOAD ACTING ON SECTIONS 1 & 2 AS A FUNCTION OF THE PITCH ANGLE θ. COMPARISON BETWEEN FILTERED EXPERIMENTAL DATA (FILT EXP, BLACK CROSSES) AND SEMI-ANALYTICAL RESULTS: FBC WITH $\lambda = 0.55$ (BLUE CIRCLE MARKS) AND CWVKM (GREEN SQUARE MARKS).

6.3 Case 3: vertical and moving cylinder ($\theta = 0$; $U_b \neq 0$)

Finally, the configuration of the vertical moving cylinder is investigated. Two surge speeds are studied, $0.4\,m.s^{-1}$ and

$0.8\,m.s^{-1}$. The position of the cylinder over time is such that the impact occurs at the same time and location for the two speeds. The cylinder speed is constant during the impact. Figure 11 represents the comparison of the load acting on each section for $U_b = 0.4\,m.s^{-1}$.

The force amplitude is lower than in the fixed configurations, especially on the impact height. The slamming force is proportional to the square of the relative velocity between the body and the fluid. The addition of a horizontal motion in the same direction as the wave propagation reduces the hydrodynamic force acting on the structure. This is an important feature that must be considered when evaluating the slamming load on FOWTs. The time variations of the load in the 4 segments are similar to that of the previous configurations without velocity.

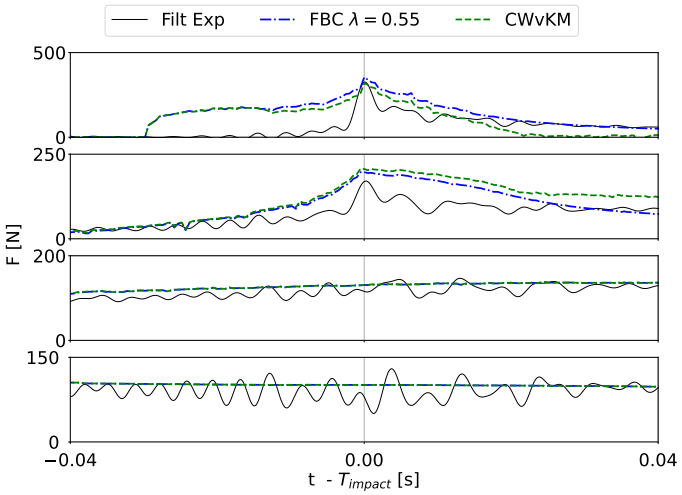

FIGURE 11: TIME HISTORY OF THE LOAD DECOMPOSED BY SECTION. FROM TOP TO BOTTOM: SECTION 1 TO 4. COMPARISON BETWEEN FILTERED EXPERIMENTAL DATA (FILT EXP, BLACK LINE) AND SEMI-ANALYTICAL RESULTS: FBC WITH $\lambda = 0.55$ (BLUE DASH-DOT LINE) AND CWVKM (GREEN DASHED LINE). - $\theta = 0$; $U_b = 0.4\,m.s^{-1}$

The maximum measured and computed load acting on the first two sections as a function of the surge speed is presented in Fig. 12. The mean relative discrepancies between the experimental data and the semi-analytical models, CWvKM and FBC, are 8% and 12%.

In all cases, both models are able to capture the maximum load acting on the cylinder. The CWvKM was developed for this purpose, without the necessity to define λ. The load increase is overestimated, mainly because of the contribution of the force acting in the upper section which is highly overestimated when the jet hits the body. The decay in load is in better agreement in sections 1 and 2 by considering flow separation, but it requires the calibration of λ.

7. DISCUSSION

7.1 Influence of λ and variation of fluid velocity

The semi-analytical model based on the FBC method relies on the parameter λ, which defines the height over which the flow separates from the structure. This parameter can be considered

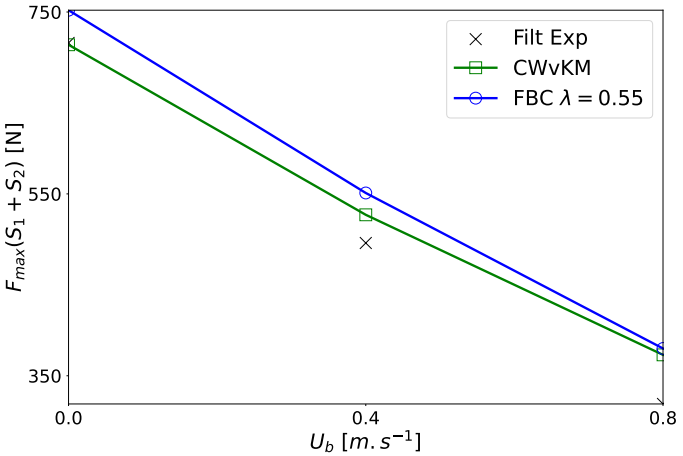

FIGURE 12: VARIATION OF THE MAXIMUM LOAD ACTING ON SECTIONS 1 & 2 AS A FUNCTION OF THE SURGE SPEED U_b. COMPARISON BETWEEN FILTERED EXPERIMENTAL DATA (FILT EXP, BLACK CROSSES) AND SEMI-ANALYTICAL RESULTS: FBC WITH $\lambda = 0.55$ (BLUE CIRCLE MARKS) AND CWVKM (GREEN SQUARE MARKS).

equivalent to the curling factor used in engineering formulas [1, 2, 4], which defines the portion of the wave contributing to the impact. Engineering formulas for breaking waves slamming load are often conservative. In [24], it is pointed out that for breaking wave impacts, the slamming coefficient is much too large. 3D effects, specifically for small curling factors, drastically decrease C_s. These simplified formulations assume that the wavefront is vertical and that the fluid velocity is uniform along the entire front. The resulting slamming force is obtained by integrating a 2D slamming load over the impact height:

$$F_s = \int_{(1-\lambda)\,\eta_b}^{\eta_b} F_{2D}\,dz = \rho R C_s \int_{(1-\lambda)\,\eta_b}^{\eta_b} U^2\,dz = \rho R C_s \lambda \eta_b C^2 \tag{5}$$

The impact load varies linearly with λ when a uniform velocity U over $\lambda\eta_b$ is accounted for. The slamming load computed with the classical simplified formulations is often highly conservative. We believe that the consideration of a uniform velocity over the impact area is at the origin of this overestimation.

As illustrated in Fig. 13, the fluid velocity rapidly decreases on the front. The free surface elevation and horizontal fluid velocity are depicted when the wavefront is vertical. The blue vertical line corresponds to the phase velocity, often used in engineering formulas. In this example, the cylinder axis is located at $21.21\,m$. The instant considered is the instant of maximum load acting on the cylinder. The free surface elevation involved in the maximum slamming force is given by the intersection of the free surface with the cylinder, here noted η_v. In this example, η_v also corresponds to the top of the vertical portion of the wavefront, and represents $0.95\eta_b$. η_v is the maximum integration height of the load. A parametric model for the horizontal speed, such as $U(z) = Cz'^2$ with $z' = z/\eta_v$, represents well the variation of the velocity with respect to the vertical axis, for this particular wave.

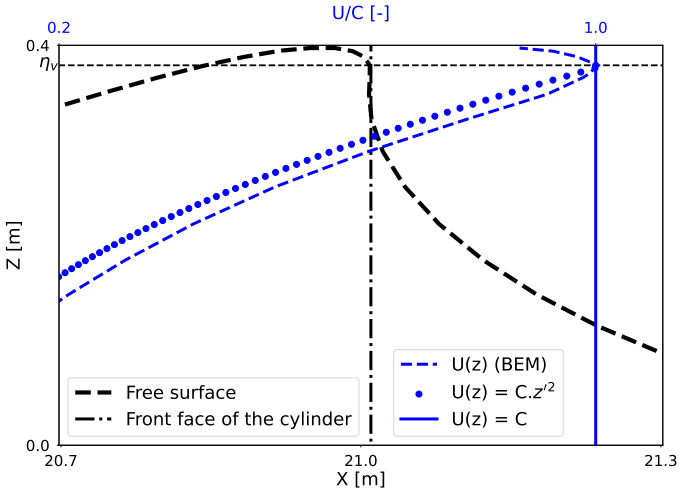

FIGURE 13: FREE SURFACE ELEVATION (BLACK DASHED LINE), FRONT FACE OF THE CYLINDER (BLACK DASH-DOT LINE) AND HORIZONTAL FLUID VELOCITY AT THE FREE SURFACE ($U(z)$ (BEM), BLUE DASHED LINE), THE PARAMETRIC MODEL ($U(z) = C.z'^2$, BLUE CIRCLES) AND THE PHASE VELOCITY ($U(z) = C$, BLUE VERTICAL LINE).

Substituting this expression into the Eq. 5, the slamming force follows:

$$F_s = \rho R C_s C^2 \int_{(1-\lambda)\eta_v}^{\eta_v} \left(\frac{z}{\eta_v}\right)^4 dz = \rho R C_s C^2 \frac{\eta_v}{5}(1-(1-\lambda)^5) \tag{6}$$

Figure 14 shows the variation of the non-dimensional force calculated by four approaches as a function of λ. The load is computed by using a simplified formulation within the frame of Wagner's theory, such as $F_s = \rho R 2\pi\lambda\eta_v C^2$ (similar to the maximum load predicted by W&O formula), with the formula proposed in [4], using Eq. 6 with $C_s = 2\pi$ and finally, the load predicted by the slamming term ($F_v U^2$) within the frame of the FBC model.

The maximum force and its evolution with λ are similar between the proposed simplified approach and the FBC-based model. The load remains nearly constant for large λ and converges to $2\pi/5$. Consequently, the maximum force depends less on λ and the overestimation of this parameter leads to a much lower difference in terms of maximum load than with the current formulas. The formulation presented in [4] accounts for an extra coefficient, $2/\pi^2$. It follows from the assessment of the pressure distribution during irregular wave slamming events on a fixed vertical cylinder. The phase-focused wave generated in our study is more severe than the waves studied in [4]. This could explain the discrepancy between this formula and the proposed approaches for small curling factors.

7.2 A new simplified formulation taking into account tilt and motion

It is assumed that the breaking wave propagates at the phase speed C. The portion contributing to the impact is defined by

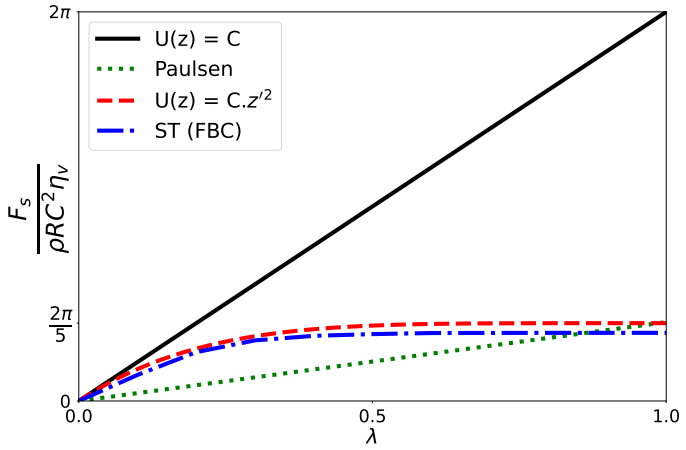

FIGURE 14: VARIATION OF THE MAXIMUM NON-DIMENSIONAL LOAD ACTING ON THE CYLINDER AS A FUNCTION OF λ. COMPARISON BETWEEN THE STANDARD FORMULATION USING A UNIFORM VELOCITY ($U(z) = C$, BLACK LINE), THE FORMULA PRESENTED IN [4] (GREEN DOTTED LINE), THE PROPOSED SIMPLIFIED FORMULATION USING THE PARAMETRIC MODEL $U(z) = C.z'^2$ (RED DASHED LINE) AND THE NON-DIMENSIONAL FORCE PREDICTED BY THE SLAMMING TERM IN THE FRAME OF THE FBC (ST (FBC), BLUE DASH-DOT LINE).

a vertical front of height $\lambda\eta_v$. The penetration depth of the wavefront in the cylinder with respect to the vertical axis can be parameterized, as depicted in Fig. 15.

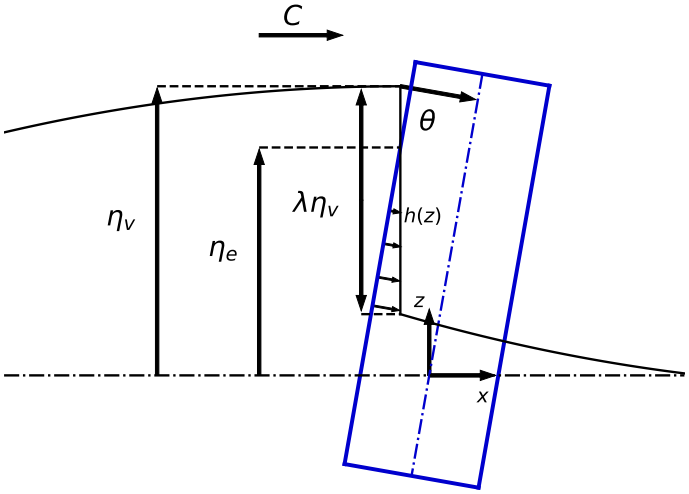

FIGURE 15: ILLUSTRATION OF THE VERTICAL WAVEFRONT IMPINGING AN INCLINED CYLINDER AND PARAMETERIZATION OF THE PENETRATION DEPTH $h(z)$.

Since the slamming coefficient depends directly on h, we elaborate a new simplified formulation accounting for the tilt of the structure. The temporal variation of h follows from the phase speed. The horizontal speed of the structure U_b is taken into account as well by considering the relative kinematics. The influence of the vertical velocity is omitted. The impact load follows:

$$F_s(t) = \rho R \int_{(1-\lambda)\eta_v}^{\eta_e(t)\leq\eta_v} C_s(h(z,t))(U(z) - U_b)^2 \cos^2\theta dz \quad (7)$$

with $\eta_e(t) = (1-\lambda)\eta_v + (C - U_b)t/\tan\theta$ ($\eta_e = \eta_v$ for $\theta = 0$) and $h(z,t) = (\eta_e(t) - z)\sin\theta$. We note T_{impact} the time at which the entire front reaches the cylinder (corresponding to the maximum impact load). At T_{impact}, $\eta_e = \eta_v$. For $t > T_{impact}$, $h(z,t) = (\eta_v - z)\sin\theta + (C - U_b)(t - T_{impact})/\cos\theta$. $C_s(h)$ is given by the FBC model. The variation of C_s with respect to h is illustrated in [10].

The formulation 7 is only valid for $\theta \geq 0$ since the height of the impact area increases (higher λ) if the cylinder is oriented towards the wave [2]. Moreover, the fluid velocity is expressed in the strip reference frame. Since the vertical velocity is directed upwards ($W > 0$), the horizontal velocity on the strip $U\cos\theta - W\sin\theta$ is higher than $U\cos\theta$ for negative θ. Thus, formula 7 would highly underestimate the slamming load.

The temporal variation of the slamming load given by Eq. 7 is compared to the experimental data in Fig. 16. The load acting on sections 1 & 2 from the configurations presented in Fig. 4, 9, 11 is depicted. λ is set to 0.55 and the slamming load from Eq. 7 is added to the quasi-static load acting on section 2 computed with the GvKM up to $(1-\lambda)\eta_v$. The maximum load as well as the load decay are in good agreement with the measurement for the three configurations. Since the wavefront is assumed to be vertical, the increase in force is instantaneous for the vertical configurations. When the cylinder is inclined, the increase is smoother as the wavefront gradually hits the cylinder.

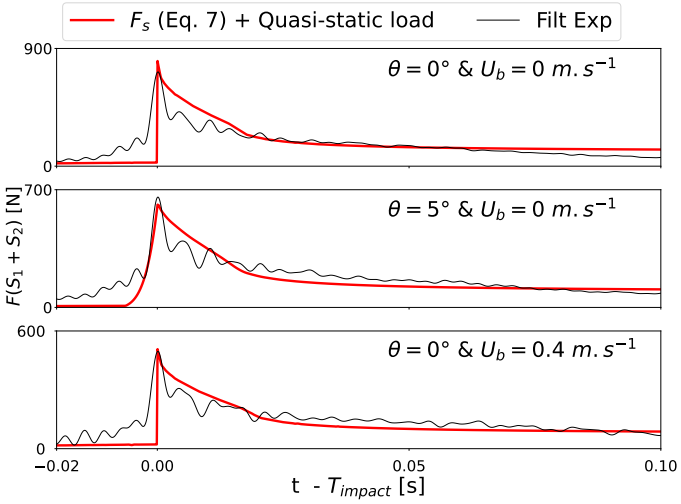

FIGURE 16: COMPARISON OF THE SLAMMING FORCE ESTIMATED BY THE SIMPLIFIED FORMULATION (F_s (EQ. 7), RED LINE) AND THE FILTERED EXPERIMENTAL DATA (FILT EXP, BLACK LINE)

8. CONCLUSION

Semi-analytical models based on Wagner's theory are implemented to capture the hydrodynamic impact load generated by a plunging breaking wave on a circular cylinder. In the CWvKM, it is assumed that the flow does not separate from the structure. Flow separation is then accounted for in a second model by using the FBC model. The nonlinear kinematics of the flow is taken into account in these models, as well as the relative motion between the body and the wave. The pitch angle of the structure is considered by projecting the fluid velocity onto the transverse direction of the strip.

A phase-focused plunging breaking wave is generated in a wave flume. A FNPF solver provides the free surface shape and kinematics of the wave. They are accounted for in a strip-theory approach under the Froude-Krylov assumption in the semi-analytical models. The load acting on the structure is then compared to the measurements obtained during the DIMPACT experimental program. Several configurations are investigated: a fixed vertical cylinder, a fixed inclined cylinder and a moving vertical cylinder. The discrepancies between the two proposed models are assessed. In general, the load impulse is overestimated, while the load decay is better predicted when modelling the flow separation. The maximum force acting on the impact height is well estimated by the two proposed semi-analytical models. However, it is important to note that the filtering of the measured signal can attenuate the actual amplitude of the peak effort. During the second experimental campaign of the DIMPACT project, a methodology based on the use of accelerometers placed on the sections will be used to compensate for the dynamic response of the sections. A higher maximum load can be expected.

A discussion regarding the influence of the parameter λ and the assumption about the fluid velocity in the engineering formulas is proposed. A simplified slamming load formulation accounting for the tilt and motion of the cylinder is developed. This new formula correctly reproduces the measured load on three configurations using simplified assumptions. It requires to define the vertical variation of the fluid velocity at the free surface. Investigations can be conducted on parametric velocity profile models to effectively utilize the proposed engineering formula for different breaking waves.

The parameter λ must be set for the FBC-based model and the new engineering formula. Since it is defined as the height at which the flow separates from the structure, it can possibly be measured from experimental video records or by evaluating the flow on Navier-Stokes simulations. A geometric and/or kinematic criterion on the undisturbed wave could then be established to estimate λ.

ACKNOWLEDGMENTS

This work is performed under financial support of grant ANR-10-IEED-0006-34, France Energies Marines project DIMPACT (Design of FOWT and IMPACTs of energetic steep and breaking waves).

REFERENCES

[1] Y. Goda, S. Haranaka, M. Kitahata, Study of impulsive breaking wave forces on piles, Report of Port and Harbor Research Institutes 5 (1966) 1–30.

[2] J. Wienke, H. Oumeraci, Breaking wave impact force on a vertical and inclined slender pile - theoretical and large-scale model investigations, Coastal Engineering 52 (2005) 435–462.

[3] E. J. Ridder, T. Bunnik, J. M. Peering, B. T. Paulsen, C. Wehmeyer, P. Gujer, E. Asp, Summary of the Joint Industry Project Wave Impact on Fixed Foundations (WIFI JIP), in: Proceedings of the ASME 2017 36th International Conference on Ocean, Offshore and Arctic Engineering, OMAE 2017, Trondheim, Norway, 2017.

[4] B. Paulsen, B. Sonneville, M. van der Meulen, N. Jacobsen, Probability of wave slamming and the magnitude of slamming loads on offshore wind turbine foundations, Coastal Engineering 143 (2019) 76–95.

[5] O. S. Madsen, Hydrodynamic force on circular cylinders, Applied Ocean Research 8 (1986).

[6] W. Manners, Hydrodynamic force on a moving circular cylinder submerged in a general fluid flow, volume 438, 1992, pp. 331,339.

[7] P. Renaud, M. Batlle Martin, F. Hulin, J. C. Harris, J.-F. Filipot, Y.-M. Scolan, Semi-analytical load models describing the progressive immersion of a fixed vertical cylinder in a breaking wave, Ocean Engineering (accepted) (2023).

[8] O. Faltinsen, Sea loads on ships and offshore structures, Cambridge University Press, 1990.

[9] M. Alagan Chella, B. H., D. Myrhaug, Wave impact pressure and kinematics due to breaking wave impingement on a monopile, Journal of Fluids and Structures 86 (2019) 94–123.

[10] A. Tassin, A. Korobkin, M. Cooker, On analytical models of vertical water entry of a symmetric body with separation and cavity initiation, Applied Ocean Research 48 (2014) 33–41.

[11] F. Hulin, A. Tassin, J.-F. Filipot, N. Jacques, Experimental investigation of the hydrodynamic loads induced by breaking wave impacts on a spar-type floating offshore wind turbine substructure, in: 18ème Journées de l'Hydrodynamique, Poitiers, France, 2022.

[12] S. Grilli, J. Skourup, I. A. Svendsen, An efficient boundary element method for nonlinear water waves, Engineering Analysis with Boundary Elements 6 (1989) 97–107.

[13] S. Grilli, R. Subramanya, Numerical modeling of wave breaking induced by fixed or moving boundaries, Comput. Mech. 17 (1996) 374–391.

[14] A. Korobkin, Analytical models of water impact, Euro. Jnl of Applied Mathematics 15 (2004) 821–838.

[15] A. Korobkin, T. Khabakhpasheva, S. Malenica, Y. Kim, A comparison study of water impact and water exit models, Int. J. Nav. Archit. Ocean Eng. 6 (2014) 1182–1196.

[16] M. Greenhow, S. Ahn, Added mass and damping of horizontal circular cylinder sections, Ocean Engineering 15 (1988) 495–504.

[17] W. Manners, R. Rainey, Hydrodynamic forces on fixed submerged cylinders, in: Proc Roy Soc Lond A Jan. 1992;436(1896):13–32., 1992.

[18] I. Campbell, P. Weynberg, Measurement of parameters affecting slamming, Technical Report, University of Southampton : Wolfson Unit for Marine Technology, 1980.

[19] X. Zhu, O. Faltinsen, C. Hu, Water entry and exit of a horizontal circular cylinder, Journal of Offshore Mechanics and Arctic Engineering 129 (2005).

[20] M. Lackner, D. Schmidt, S. Arwade, A. Myers, A. Robertson, Simulating breaking waves and estimating loads on offshore wind turbines using computational fluid dynamic models, Technical Report, University of Massachusetts Amherst, 2018.

[21] A. Nestegård, K. Hagatun, S. Haver, A. Kalleklev, Y. Wu, E. Lehn, Resonant vibrations of riser guide tubes due to wave impact, in: 23rd International Conference on Offshore Mechanics and Arctic Engineering, 2004. doi:DOI 10.1115/OMAE2004-51545.

[22] L. Suja-Thauvin, E. Bachynski, F. Pierella, M. Borg, J. Krokstad, H. Bredmose, Critical assessment of hydrodynamic load models for a monopile structure in finite water depth, Marines Structures 72 (2020).

[23] M. Batlle Martin, J. C.Harris, P. Renaud, F. Hulin, J.-F. Filipot, Numerical investigation of slamming loads on floating offshore wind turbines, in: Proceedings of the 32nd International Offshore and Polar Engineering Conference, Shanghai, China, 2022.

[24] A. Ghadirian, F. Pierella, H. Bredmose, Calculation of slamming wave loads on monopiles using fully nonlinear kinematics and a pressure impulse model, Coastal Engineering 179 (2023) 76–95.